

Frequency Management of an Interconnected Power System using Modified Differential Evolution Algorithm

Debayani Mishra*^{ID}, Manoj Kumar Maharana**[‡]^{ID}, Manoj Kumar Kar***^{ID}, Anurekha Nayak****^{ID}

* Research Scholar, School of Electrical Engineering, KIIT Deemed to be University, Bhubaneswar, Odisha

** Associate Professor, School of Electrical Engineering, KIIT Deemed to be University, Bhubaneswar, Odisha

*** Senior Assistant Professor (Electrical Engineering), Tolani Maritime Institute Talegaon, Maharashtra

**** Associate Professor, DRIEMS, Cuttack, Odisha

(debayanim@gmail.com, mkmfel@kiit.ac.in, manojkar132@gmail.com, anurekha2611@gmail.com)

[‡]Corresponding Author; Debayani Mishra, School of Electrical Engineering, KIIT Deemed to be University, Bhubaneswar

Tel: +91 9438636980,

debayanim@gmail.com

Received: 21.10.2022 Accepted: 09.12.2022

Abstract- In recent decades, microgrid systems have included renewable energy sources due to insufficient power generation. However, uncertainty in the output of renewable sources and load change have an effect on the system frequency, affecting the microgrid's ability to operate reliably. For continuous electric power, an intelligent controller is essential to improve system stability. This paper proposes the construction of a cascaded Modified Differential Evolution (MDE)-based PIDFN controller utilizing ITAE. The suggested MDE tune PIDFN controller is compared to IPD-(1+I) and PI controller to illustrate its robustness and effectiveness. Implementation of an MDE-based cascaded PIDFN controller for frequency regulation in a two-area linked microgrid system. In a MATLAB®/SIMULINK environment, the system is validated across load perturbations, system uncertainties, communication latency, real-time data on solar irradiance and wind speed, and the action of UPFC. The effectiveness of the MDE-PIDFN controller is also analyzed statistically.

Keywords Modified Differential Evolution, Differential Evolution, IPD-(1+I), Cascaded-PIDFN.

1. Introduction

In the past years the generation of power has transitioned from conventional fossil fuel based thermal power plants to power generating units comprising of renewable sources situated nearer to the consumer. This configuration is termed as microgrid which further minimizes the transmission losses of the system and facilitates a better control and satisfies the power requirement. The sporadic nature of renewable sources employed in microgrid leads to significant deviation in system frequency and tie line power variation from its specified value. In order to get the system's frequency closer to its nominal values, it is necessary to integrate these energy sources with improved control techniques for power generation. Therefore, load frequency control is essential for reliable and stable operation of power system.

The LFC plays an integral role ensuring the stability of the microgrid system during load fluctuations and variations of renewable sources. In literature the frequency of the power system was controlled by robust optimal[1], stochastic

optimal[2], and secondary control methods [3],[4]. Sliding mode controllers are implemented for frequency control in an isolated microgrid[5],[6]. In addition, it provides good power sharing among distributed generation (DGs) and also offers accurate active and reactive power distribution[7]. The controller settings are fine-tuned precisely to obtain an improved LFC response. In this reference, several meta-heuristic techniques like teaching learning-based optimization (TLBO)[8] artificial bee colony[9], ant-lion optimization[10], grey wolf[11], genetic[12], bacterial foraging[13],[14], whale optimization[15], ant colony[16],[17] etc are proposed in literature that yields a global optimum. However, these optimization strategies did not yield enhanced performance in terms of settling time, peak overshoot or peak undershoot. In[18],[19] Differential Evolution (DE) search approach was able to efficiently handle optimization challenges. In a particular method, the performance of DE depends on the values chosen for the crossover constant and scaling factor. In this research, a strategy called Modified Differential Evolution (MDE) is

proposed to solve DE's shortcomings. It has been investigated in the literature that the performance of an LFC system does not depend just on its optimization approach, but also on its controller architecture. Diverse controllers, including adaptive control[20],[21] and model predictive control [22],[23] have been proposed to regulate the frequency in an isolated MG system. In[24], internal model (IMC) tuned PI controller and fractional order PI controller (FOPI) has been designed to improve the frequency regulation of a microgrid. The proposed approach outperforms better in comparison to Ziegler Nichols method. A hybrid power flow controller is designed in [25] that regulates the active power generated by PV inverter and a diesel generator as a function of system frequency. The proposed controller demonstrates a better performance when the system was subjected to abrupt change in load. In literature the author has analyzed demand side management [26]as a new control mechanism for regulating the frequency of the microgrid implementing PI and PID controller using evolutionary method firefly algorithm (FA). Due to the erratic nature of RES, these traditional controllers [27],[28] fail to function properly under diverse operating situations. In contrast, fractional order controllers[29], which increase the stability of an interconnected MG system, have received a significant lot of attention in recent years due to their adaptable structure and larger number of tuning parameters. In recent years, cascaded controllers [30] have been utilized in linked power systems because they can successfully endure a variety of disruptions. In this regard, a cascaded PIDFN controller is proposed for an interconnected microgrid system in order to reduce frequency disturbances.

1.1 Research Gap and Motivation

Classical controllers, such as P, PI, and PID, are efficient for hybrid MG systems. In terms of parameter modifications, these controllers are slow in response to sudden load disturbances. Additional sliding mode controllers, fractional order PI controllers, and PID controllers have structural flaws and require additional expenses. These results support the creation of a cascaded PIDFN controller. It is a combination of PIDN controller and PIDFN controller that utilizes a fractional order filter to solve the realizability problem. The recommended controller is more effective in reducing frequency variations in the system.

This study, inspired by previous research, proposes an MDE approach for tweaking the parameter of the cascaded-PIDFN controller[31]. In terms of ITAE and convergence, the offered optimization strategies surpass previous optimization methods.

1.2 Contribution and Paper Organization

The following are the contributions and characteristics of the proposed work:

1. A distinctive Modified Differential (MDE) technique is utilized to update the cascaded PIDFN controller's parameter.
2. The superiority of the MDE tuned PIDFN algorithm demonstrated by comparing it with PI and IPD both tuned by MDE.

3. The performance of the proposed cascaded PIDFN controller is examined under various conditions, including dynamic load disturbance, system uncertainties, communication latency, and real-time measurements of sun irradiance and wind speed. In a MATLAB/SIMULINK environment, the actions of the unified power flow controller (UPFC) are also evaluated on a two-area linked microgrid system.

The structure of the paper is as follows: The second section explains the model of the hybrid renewable energy system (HRES), while the third portion examines the cascaded PIDFN controller. In Section 4, the performance of the MDE is addressed, and in Section 5, simulation results are shown. Section 6 provides the performance in terms of ITAE value and conclusion is presented in Section 7.

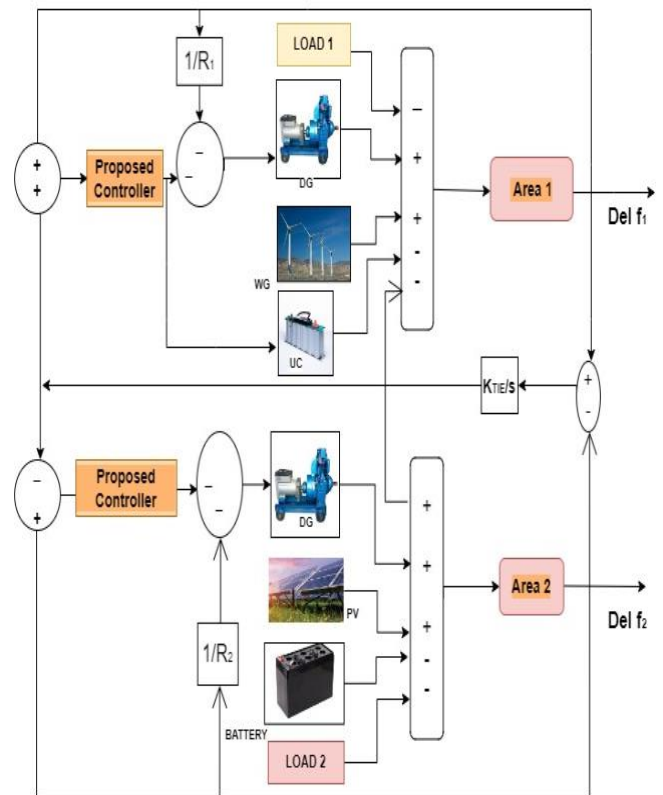


Fig.1. Proposed MG system

2.1. Modelling of PV System

The PV system generates variable electricity due to erratic nature of solar radiation and temperature. The, power obtained from the PV cell [32] is determined using equation

$$P_{PV} = \eta S \Phi (1 - 0.005(T_a + 25)) \tag{1}$$

where η = effectiveness of PV array

S = PV Surface area

ϕ = Intensity of Solar radiation

T_a = Surrounding temperature

2.2. Modelling of Wind Turbine System

Variable wind speed causes the wind turbine's output power to be erratic. The WG is characterized as a combination of power coefficient 'C_p' and other physical factors tip speed ratio 'λ' and blade pitch angle 'β' are the fundamental components of 'C_p'. The output mechanical power of the WG is expressed in equation (2) as follows

$$P_{WG} = \frac{1}{2} \rho A C_p V_w^3 \tag{2}$$

where A is the area covered by the turbine blades in m³
 ρ is the density of air in kg/m³

2.3. Modelling of the Diesel Engine Generator Units

The diesel engine generator (DG) is well-known in the MG system as an efficient source of power that functions with remarkable durability and efficiency during load augmentation. The DG transfer function model is represented in Figure 2. The valve actuator controls diesel engine output power

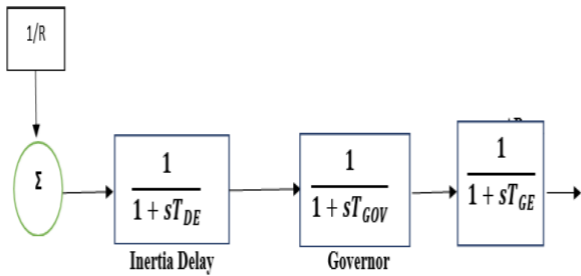


Fig.2. Block diagram of DG

2.4 Modelling of Battery Energy System

The DEG sources have a low response time, thus they are augmented by energy storage devices to better frequency control. The battery energy system (BES) functions as storage units, and frequency variations are maintained by exchanging power with the microgrid. The transfer function model of BES system is represented in equation (3) as

$$G_{BES}(s) = \frac{K_{BES}}{1 + sT_{BES}} \tag{3}$$

2.5 Modelling of Ultracapacitor

It is a charged electrostatic component. In contrast to batteries, it can last thousands of cycles. Significantly quicker charging and draining times have been implemented for the storage units. It features minimal resistance and rapid response to power fluctuations. The transfer function is given in equation (4) as

$$G_{UC}(s) = \frac{1}{1 + sT_{UC}} \tag{4}$$

2.6 Modelling of Microgrid System

All sources supply energy, and a correlation between frequency variation and energy consumption is established. The transfer function model is represented in equation (5) as

$$\frac{\Delta F}{\Delta P} = \frac{K_{PS}}{1 + sT_{PS}} \tag{5}$$

The microgrid component is assumed to be linear and modelled with a first-order transfer function in the MATLAB®/SIMULINK environment, as shown in Table 1.

Table 1: Parameters of the microgrid model

	Transfer Function	Gain	Time Constant
DG	$\frac{K_{DG}}{1 + sT_{DG}}$	$K_{DG} = 0.03$	$T_{DG} = 2$
WG	$\frac{K_{WG}}{1 + sT_{WG}}$	$K_{WG} = 1$	$T_{WG} = 0.05$
PV	$\frac{K_{PV}}{1 + sT_{PV}}$	$K_{PV} = 1$	$T_{PV} = 0.03$
UC	$\frac{1}{1 + sT_{UC}}$		$T_{UC} = 0.08$
Synchronizing Coefficient	$\frac{K_{TIE}}{s}$	$K_{TIE} = 0.56$	
BES	$\frac{K_{BES}}{1 + sT_{BES}}$	$K_{BES} = -0.03$	$T_{BES} = 0.1$
Droops	R_1, R_2	$R_1 = R_2 = 0.05$	
Power System	$\frac{K_{PS}}{1 + sT_{PS}}$	$K_{PS} = 120$	$T_{PS} = 20$

3. Modified Differential Evolution

The Differential Evolution algorithm is introduced by Storn in 1997, consists of four steps: (i) initialization (ii) mutation (iii) crossover (iv) selection. In literature it has been observed that DE is simpler, easier to build, and has less variables than typical evolutionary algorithms. In the first step, n numbers of population size and decision vectors are selected randomly as follows $\vec{X}_k^l = (X_1^l, X_2^l, \dots, X_D^l)$ over D-dimensional search space. In second step, a mutant vector \vec{M}_k^l is formulated by applying the mutation operator any of the following equations (6) to equation (10)

$$DE/rand/1: \vec{M}_k^l = \vec{X}_{k1}^l + f(\vec{X}_{k2}^l - \vec{X}_{k3}^l) \tag{6}$$

$$DE/best/1: \vec{M}_k^l = \vec{X}_{best}^l + f(\vec{X}_{k1}^l - \vec{X}_{k2}^l) \tag{7}$$

DE/rand/2:

$$\vec{M}_k^l = \vec{X}_{k5}^l + f(\vec{X}_{k1}^l - \vec{X}_{k2}^l) + f(\vec{X}_{k3}^l - \vec{X}_{k4}^l) \tag{8}$$

DE/best/2:

$$\vec{M}_k^l = \vec{X}_k^l + f(\vec{X}_{k1}^l - \vec{X}_{k2}^l) + f(\vec{X}_{k3}^l - \vec{X}_{k4}^l) \quad (9)$$

DE/current-to-best/1:

$$\vec{M}_k^l = \vec{X}_k^l + f(\vec{X}_{best}^l - \vec{X}_k^l) + f(\vec{X}_{best}^l - \vec{X}_{k2}^l) \quad (10)$$

In third step, the decision vector (\vec{X}_k^l) and mutant vector (\vec{M}_k^l) undergo crossover operation to form a trial vector (\vec{V}_{ij}^l), expressed in equation (11) as

$$V_{kj}^l = \begin{cases} M_{kj}^l & \text{if } rand(0,1) < Cr \\ X_{kj}^l & \text{otherwise.} \end{cases} \quad \text{for } j = 1, 2, \dots, D \quad (11)$$

In last step, the vector for the subsequent generation is selected considering the expression in equation (12) as

$$X_k^{l+1} = \begin{cases} V_k^l & \text{if fitness of } V_k^l \text{ is better than } X_k^l \\ X_k^l & \text{otherwise} \end{cases} \quad (12)$$

Where, \vec{X}_k^l is the kth decision vector of lth generation
 \vec{M}_k^l is the kth mutant vector of lth generation
 \vec{X}_k^l and \vec{X}_{best}^l are the lth generation's randomly chosen decision vector and best solution vector respectively
 f and Cr are the scale factor and crossover rate respectively whose value ranges between 0 and 1.

The DE/best mutation operator has more exploitation features than exploration and produces optimum solutions faster. This method, however, is susceptible to early convergence and local optima. A novel mutation operator is presented in this paper known as Modified Differential Evolution (MDE) algorithm to prevent this difficulty and maintain a balance between exploitation and exploration. Here, six best solutions from the current generation are chosen to find three mutant vectors equation (13) to equation (15). The final mutant vector (\vec{M}_k^l) is then calculated by taking the average of these three mutant vectors. In crossover step, a new trial vector is obtained as per equation (16). Finally, in selection step, the decision vector for next generation is obtained as expressed in equation (17)

$$\vec{M}_1 = \vec{X}_k^l + f(\vec{X}_{best1}^l - \vec{X}_k^l) + f(\vec{X}_{best2}^l - \vec{X}_k^l) \quad (13)$$

$$\vec{M}_2 = \vec{X}_k^l + f(\vec{X}_{best3}^l - \vec{X}_k^l) + f(\vec{X}_{best4}^l - \vec{X}_k^l) \quad (14)$$

$$\vec{M}_3 = \vec{X}_k^l + f(\vec{X}_{best5}^l - \vec{X}_k^l) + f(\vec{X}_{best6}^l - \vec{X}_k^l) \quad (15)$$

$$\vec{M}_k^l = Mean(\vec{M}_1, \vec{M}_2, \vec{M}_3) \quad (16)$$

$$f = 2X(1 - \frac{l}{L_{max}}) \quad (17)$$

Where $\vec{X}_{best1}^l, \vec{X}_{best2}^l, \vec{X}_{best3}^l, \vec{X}_{best4}^l, \vec{X}_{best5}^l$ and \vec{X}_{best6}^l are the six best decision vectors chosen from lth generation and L_{max} are the current and maximum generation respectively. The flow chart related to MDE algorithm is described in Figure.4 as follows

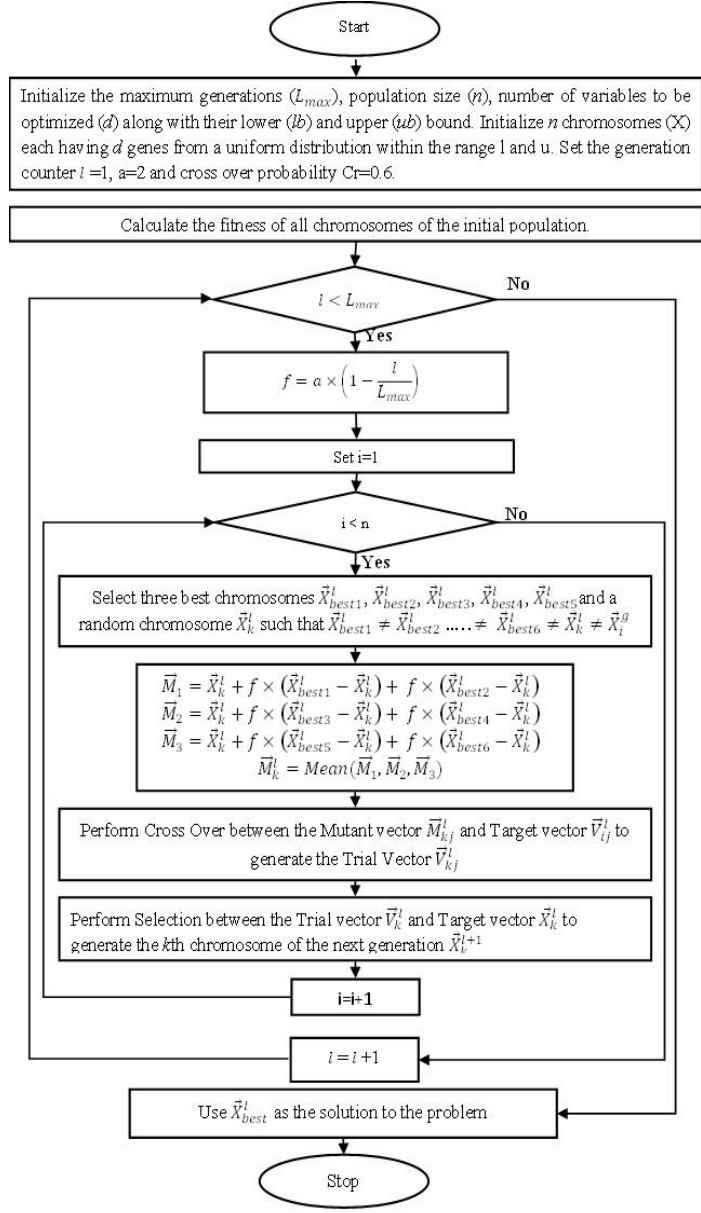


Fig.4. Flowchart of MDE

For comparing the performance of MDE algorithm with respect to DE, PSO, TLBO and IWO the convergence curve is represented in Figure 5. Each methodology procedure is assessed using 100 iterations, using 20 search agents or members of the population. The proposed method is validated by applying it to established benchmark test functions[33]. The Friedman and Nemenyi hypothesis test are used to score the thirteen-benchmark unimodal and multimodal optimization algorithms represented in Table.2.

The suggested MDE approach performs better in F1, F2, F3, F5, F6, F8, F9, F10, F11, F12 and F13 benchmark functions as compared to other optimization methods such as DE, IWO, TLBO and PSO. In benchmark function F4 and F7 the DE has a better performance.

4.Controller Structure

The primary objective of the proposed controller architecture [34] is to manage the frequency response of the hybrid microgrid system in response to rapid load disruptions and/or RES variations. A cascaded-PIDFN controller is suggested in each area of the to regulate the frequency variations ΔF_1 and ΔF_2 and minimize tie line power deviations ΔP_{tie} . The proposed controller is a cascaded design of PID controller with filter parameter (PIDN) and a fractional order PID controller with an integer filter (PIDFN) based on fractional calculus and including differentiators and integrators represented in Figure 5.

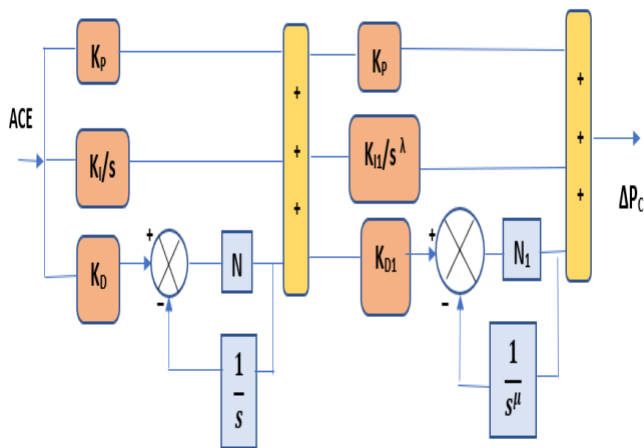


Fig.5. Proposed Controller Structure

The PIDN controller consists of a P, I, and D controller with a derivative filter coefficient N, whereas the PIDFN controllers have the form of PI, λ , D, μ with a derivative filter coefficient N. λ and μ are the order of integrators and differentiators is and. With the addition of a fractional order PIDN controller, the integer order PIDN controller may be expanded from point to plane, hence making the PIDN control approach more adaptive and resilient. The controller PIDN is a typical form of derivative filter PID controller and can be written as in equation (18) as

$$G_{PIDN}(s) = K_p + \frac{K_I}{s} + K_D \left(\frac{sN}{s+N} \right) \tag{18}$$

The Area Control Error (ACE) is the input to the controller the output of the PIDFN controller is fed to a fractional order PIDN controller governed by the equation (19) as

$$G_{PIDFN}(s) = K_{P1} + \frac{K_I}{s^\lambda} + K_{D1} \left(\frac{s^\mu N}{s^\mu + N} \right) \tag{19}$$

The scaling parameters provided by the advanced control optimization, the gain parameters of a cascaded PIDFN controller become more flexible. Further the performance of

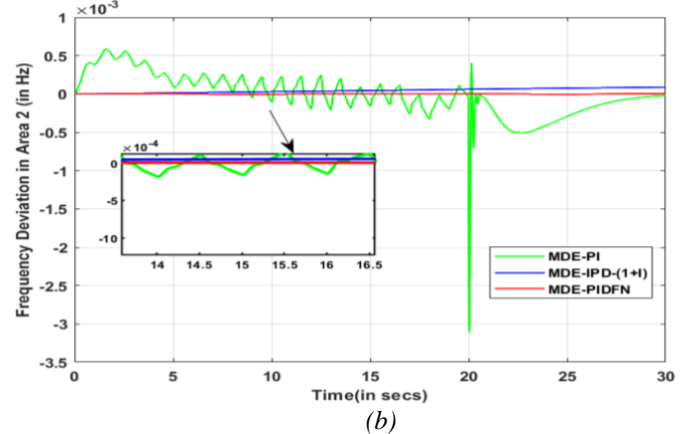
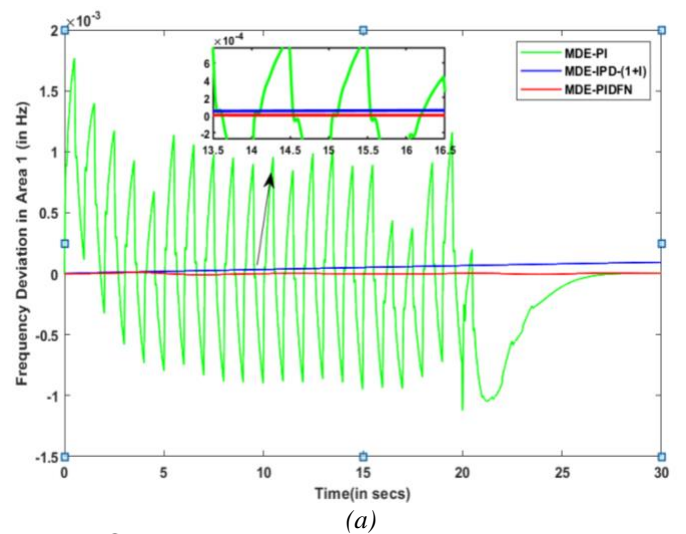
the proposed controller is compared with the conventional PI and IPD-(1+I) controller tuned by MDE optimization strategy.

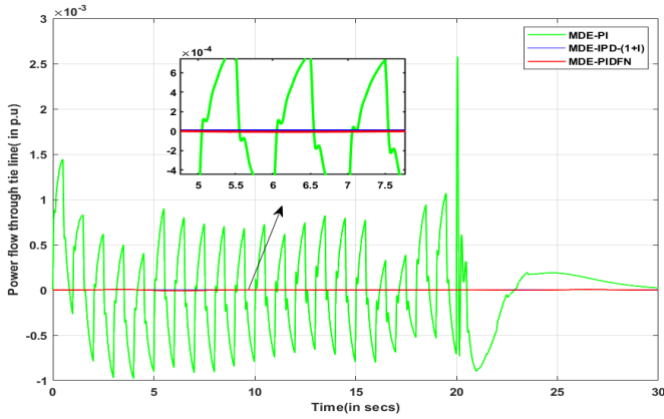
5.Results and Discussion

In this section, the HRES is tested under a variety of conditions, including step load perturbations in both the areas, incorporation of FACTS devices in the hybrid system with real-time solar irradiance and wind speed data, communication latency, and parameter variations. To exemplify the efficacy of the proposed method, its simulation results in the time domain are compared with those of certain well-studied algorithm [30]. In each case the MDE-PIDFN is compared with MDE-IPD-(1+I) and MDE-PI. The comparison is based on ITAE and dynamic values of ΔF_1 , ΔF_2 and ΔP_{tie} . The population size, swarm size, or number of search agents in all meta-heuristic algorithms is set at 20 and executed up to 100 iterations.

5.1 Step Load Disturbances

In this scenario, the system is subjected to 2% step load disturbance both in Area 1 and Area 2. The frequency and tie line power deviations of area 1 and area 2 are represented in Figure 6(a)-(c) respectively.





(c)

Fig. 6. Dynamic Response under step load disturbance (a) ΔF_1 (b) ΔF_2 and (c) ΔP_{tie}

From Figure 6(a) –6(c) it is observed that the proposed cascaded PIDFN controllers utilizing the MDE approach in area 1, area 2 and tie line has the ability to dampen transient frequency oscillations when compared to traditional controllers PI and IPD(1+I). By adopting MDE-PIDFN strategy, the settling time (ST) has improved to 17.8%, 15.38% and 16.66% in area 1, area 2 and tie line. It also exhibits a better Peak Overshoot (POS) as compared to other MDE-PI and MDE-IPD-(1+I) summarized Table 3 as follows.

Table 3:-Transient specifications under step load disturbance

Controller		MDE-PI	MDE-IPD-(1+I)	MDE-PIDFN
ΔF_1	POS	0.02	0.00015	0.00001
	TS	28	Oscillatory	23
ΔF_2	POS	0.0005	0.00025	0.000005
	TS	26	Oscillatory	22
ΔP_{tie}	POS	0.0015	0.000005	0.000005
	TS	30	Oscillatory	25

In terms of settling time, the MDE -PIDFN method provides superior dynamic responsiveness compared to other controllers.

5.2 Effect of variation of RES and action of UPFC in the system

In this case, UPFC is incorporated in the system, and the microgrid is exposed to real-time data indicating the fluctuation of PV irradiance and wind speed on a particular day, represented in Figures 7 and 8, respectively.

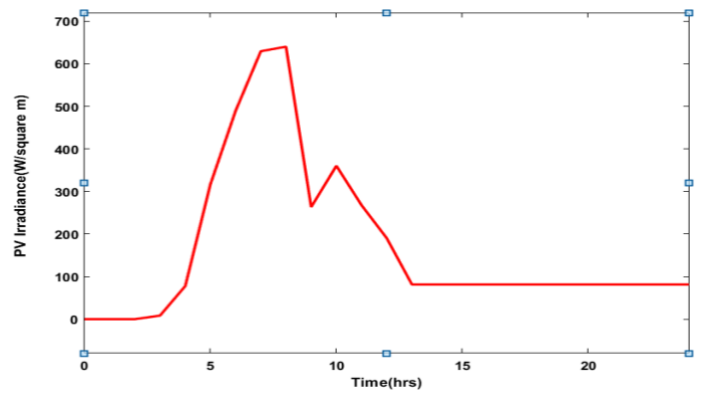


Fig. 7. Variation in PV irradiance

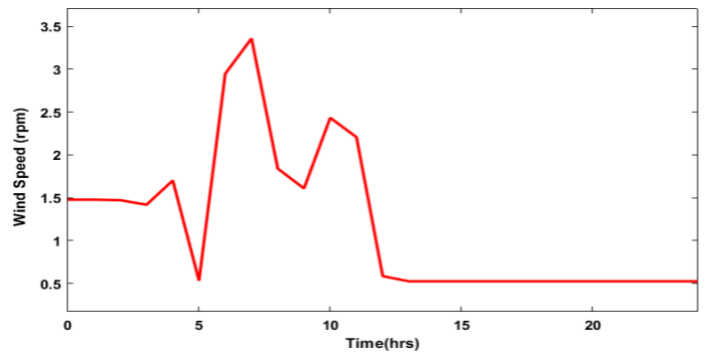


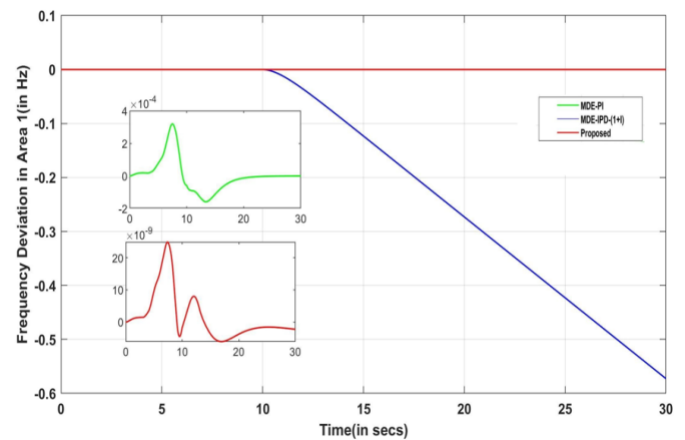
Fig. 8. Variation in wind speed data

The FACTS components increase transient stability, manage power flow, and offer voltage support, as shown in the literature. In addition, it helps to improve both the dynamic and steady-state system performance. The transfer function characterizes the UPFC is represented by equation (20)

$$G_{UPFC}(s) = \frac{1}{1 + sT_{UPFC}} \tag{20}$$

Where T_{UPFC} is the time constant i.e., 0.01 secs

The suggested coordinated controller action on the frequency stability in both the areas and tie line implementing UPFC is represented in Figure 9 (a) - 9 (c).



(a)

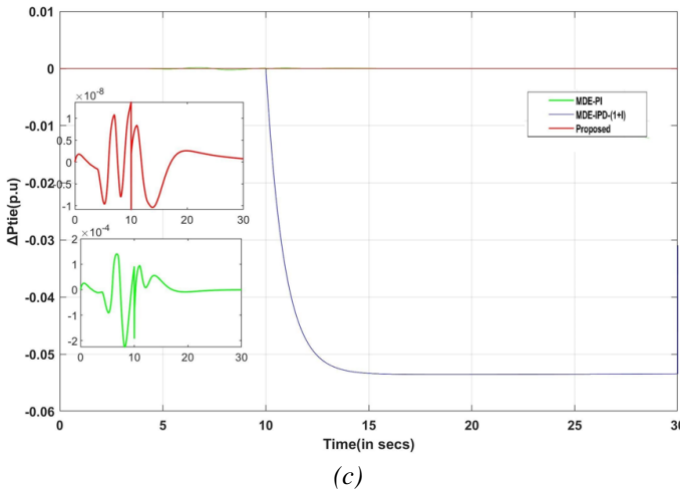
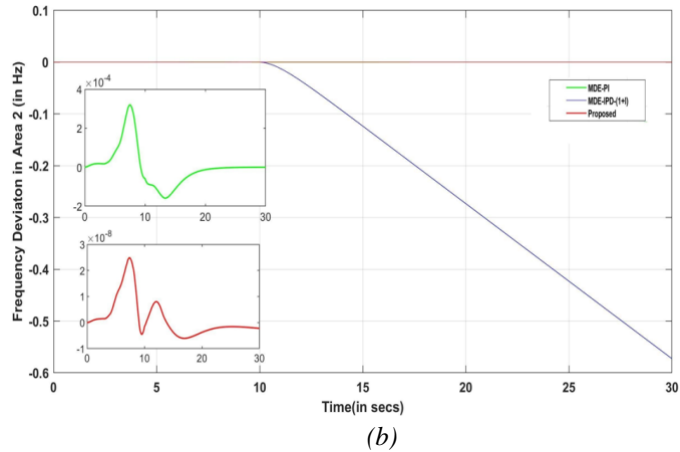


Fig. 9. Dynamic Response under fluctuations of RES (a) ΔF_1 (b) ΔF_2 and (c) ΔP_{tie}

From Figure 9 (a) it is observed that the proposed MDE-PIDFN controller represented in the zoomed figure attains a better performance as compared to other controllers. Similarly in Fig 9(b) and 9(c) proposed controller possess a better performance in both Area 2 and the tie line. The transient specification in terms of Settling Time (ST) and Peak Overshoot (POS) is represented in Table 4 as follows. The settling time improves to 12% and 3.7% using the proposed MDE-PIDFN controller as compared to MDE-PI controller.

Table 4: - Transient specifications under fluctuations of RES

Controller		MDE-PI	MDE-IPD-(1+I)	MDE-PIDFN
ΔF_1	POS	0.000033	-	0.00000002
	TS	25	26	22
ΔF_2	POS	0.00001	-	0.00000001
	TS	27	Oscillatory	26
ΔP_{tie}	POS	0.000025	-	0.00000001
	TS	22	26	25

5.3 Robustness of the Controller

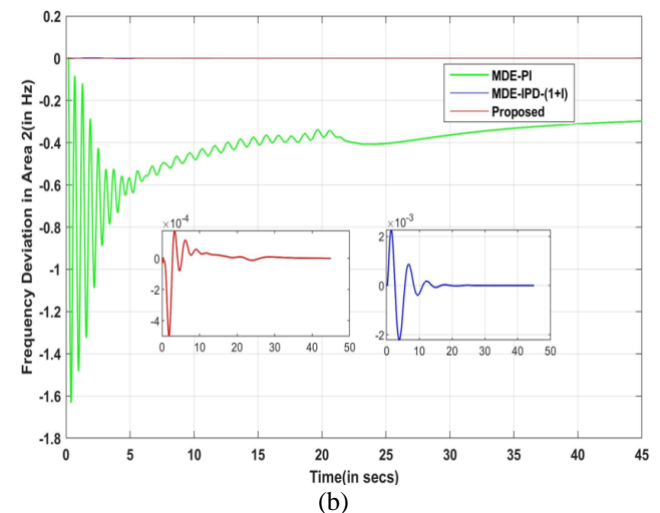
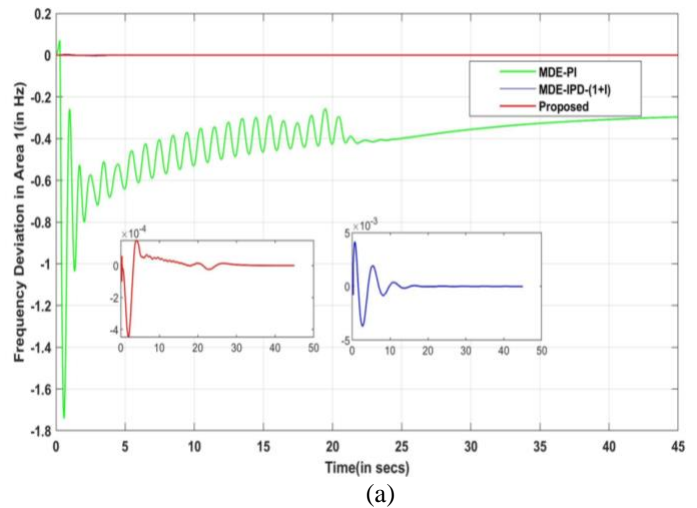
In order to investigate the robustness of the proposed controller the system is subjugated to parametric variations

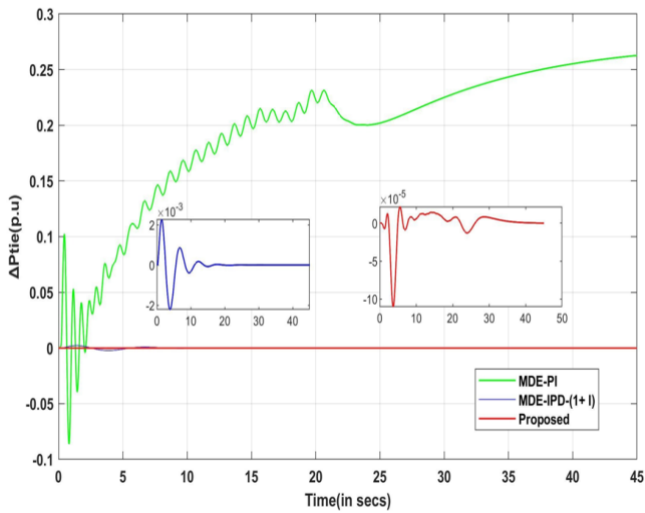
in the system depicted in Table 5 and communication delay at time 0.1 secs is implemented at the input of each controller in both the areas. It is studied in literature that the CTDs reduce system instability, hence their effect on frequency stability is investigated here. In addition, area 1 experiences a step load shift at 30 seconds and area 2 at 20 seconds shown in Figure 10.

Table 5: - Parameter Variation

	Parameter	Variation (in %)
Area 1	R	+ 5
	D	-20
	H	+25
Area 2	R	-5
	D	+20
	H	-25

Figures 10(a)-10(c) represents the dynamic response of frequency deviations F_1 and F_2 in Area 1 and Area 2 respectively, as well as the tie line power variation of ΔP_{tie} .





(C)
Fig. 10. Dynamic response under parameter variations (a) ΔF_1 (b) ΔF_2 and (c) ΔP_{tie}

From Figure 10 (a)-10(c) it is observed that the suggested controller represented in the zoomed portion of the figure offers enhanced dynamic responsiveness in terms of settling time and peak overshoot. The transient specifications of the system are represented in Table 6.

Table 6:- Transient specifications under parameter variation

Controller		MDE-PI	MDE-IPD-(1+I)	MDE-PIDFN
ΔF_1	POS	1.74	0.00806	0.000447
	TS	Oscillatory	33	30
ΔF_2	POS	1.63	0.0015	0.000496
	TS	Oscillatory	37	36
ΔP_{tie}	POS	0.084	-	0.00000073
	TS	Oscillatory	34	33

In terms of a noticeable reduction in settling time and overshoot, the suggested MDE-PIDFN controller displays improved dynamic performance compared to MDE-PI and MDE-IPD-(1+I) controllers as explained in Table 6. The settling time is improved to 9.09%, 2.7% and 2.9% in area 1, area 2 and tie line as compared to MDE-IPD-(1+I) controller.

6.Performance Comparison

The performance indices in terms of ITAE for the controllers under all test scenarios are studied in Table 7. It, demonstrates that the suggested controller can obtain greater values of performance indices in a variety of system configurations. Furthermore, the analyzed performance indices demonstrate that the suggested controller is better than conventional controllers.

Table 7: -Comparative analysis of ITAE for different scenarios

Scenario	Controller	ITAE
1	MDE-PI	0.61027
	MDE-IPD-(1+I)	0.002418
	MDE-PIDFN	0.00095
2	MDE-PI	0.0236
	MDE-IPD-(1+I)	0.000006
	MDE-PIDFN	0.000003
3	MDE-PI	0.002
	MDE-IPD-(1+I)	0.26802
	MDE-PIDFN	0.0038

7. Conclusion

In this work difficulties associated with load frequency control for an interconnected microgrid system is addressed. Using the DE optimization strategy as a basis, an intelligent optimization technique MDE is developed for efficient frequency control of the proposed system. The proposed optimization stratagem MDE exhibits a better convergence as compared with DE, PSO, TLBO and IWO and the proposed strategy. By reducing ITAE performance indices, the suggested method was utilized to optimize the cascaded-PIDFN controller's settings. In order to determine the efficacy of the proposed controller, the microgrid system is exposed to load perturbation, parametric fluctuations, and the influence of CTD and UPFC in the system. The settling time (frequency deviation in area1, frequency deviation in area2, power flow through tie line) during fluctuation of RES were 22 sec,26 sec and 25 sec against 25 sec,27 sec and 26 sec using MDE-PI controller. The proposed controller attains a better settling time, peak overshoot and peak undershoot as compared to other controllers. In accordance with extension to the research work newly proposed algorithm methods can be used to tune the cascaded the PIDFN controller.

Table 2- Statistical Analysis of unimodal [F1-F7] and multimodal [F8-F13] benchmark functions for various algorithm

Fitness Function	Optimal Range	Methods	Best Value	Worst Value	Average	Std. Dev.
------------------	---------------	---------	------------	-------------	---------	-----------

F1	[-100, 100]	MDE	4.67325E-21	7.36249E-19	7.41065E-20	1.84564E-19
		DE	3.19308E-18	2.50005E-16	3.92307E-17	6.13443E-17
		IWO	5.41196E-14	1.35497E-11	5.07432E-12	9.2243E-12
		TLBO	1.87765E-10	1.07595E-08	1.93329E-08	3.00768E-08
		PSO	3.27634E-23	1.52175E-18	9.97963E-19	1.92524E-18
F2	[-10,10]	MDE	2.5799E-21	2.27222E-16	3.32188E-17	7.1224E-17
		DE	1.15444E-15	6.06036E-12	6.11851E-13	1.53958E-12
		IWO	1.3563E-09	8.42649E-08	1.50991E-08	2.32284E-08
		TLBO	3.87199E-06	9.30139E-05	2.3306E-05	2.79559E-05
		PSO	1.53289E-12	2.10691E-11	7.06776E-12	9.73929E-12
F3	[-100, 100]	MDE	1.80578E-05	0.013169206	0.001881839	0.003038376
		DE	4.50007E-07	0.435407951	0.079491579	0.147822886
		IWO	0.051642	5.568669156	1.050830336	1.478810743
		TLBO	0.719156293	146.5377069	16.03877072	41.17533
		PSO	0.00308444	0.502369032	0.08098993	0.124014843
F4	[-100, 100]	MDE	7.5742E-06	6.244365507	0.641335795	1.68452407
		DE	0.573384138	10.63719177	3.281509352	3.109980982
		IWO	1.371978527	5.704620842	4.073516258	2.002958397
		TLBO	1.878070812	10.66721955	8.380261679	9.062822052
		PSO	9.20697E-05	0.005370896	0.001790662	0.001725102
F5	[-30, 30]	MDE	0.0001369	0.226226036	0.172034028	0.1270417
		DE	7.369E-05	8.6827189	5.717675727	3.31392042
		IWO	0.625755185	22.11125307	8.004449434	6.208061902
		TLBO	4.101560219	18.42666145	8.808348811	4.931876443
		PSO	0.783659557	8.956941816	5.980186905	1.964758184
F6	[-100, 100]	MDE	3.53783E-24	4.04927E-20	2.2988E-20	3.53592E-20
		DE	2.93589E-20	1.39983E-15	1.73617E-15	4.81027E-15
		IWO	1.20189E-13	3.52501E-10	2.72436E-11	9.00824E-11
		TLBO	4.25199E-09	1.31591E-06	1.78503E-07	3.29423E-07
		PSO	7.20828E-21	1.05491E-19	3.61788E-20	2.71663E-20
F7	[-1.28, 1.28]	MDE	0.001299404	0.007578856	0.003693428	0.001798172
		DE	0.018977644	0.011787371	0.006983694	0.004492404
		IWO	0.008674623	0.054827378	0.02009956	0.01516941
		TLBO	0.049448363	0.009650135	0.026380274	0.016937231
		PSO	0.001073927	0.006027303	0.002973244	0.001421106
F8	[-500, 500]	MDE	-4189.828873	-3634.997315	-3902.134464	162.8825118
		DE	-3716.075534	-2963.17176	-3460.999726	310.1334398
		IWO	-3615.85714	-2566.582108	-3185.836073	279.2072213
		TLBO	-3521.219785	-2879.364174	-3167.847263	263.6262651
		PSO	-2669.80172	-1820.8637	-2260.40686	317.9985107
F9	[-5.12, 5.12]	MDE	1.989922905	12.93445767	6.898606289	3.06583145
		DE	2.001720939	12.93460021	7.25617983	3.249498935
		IWO	4.974795285	19.89916099	15.25601499	6.910324562
		TLBO	9.949585533	53.79864477	26.4753068	13.1293588
		PSO	8.954626476	30.84365511	14.19473308	6.207428285
F10	[-32, 32]	MDE	2.07567E-12	1.01996E-10	3.56242E-11	3.80376E-11
		DE	2.36579E-08	1.94939E-06	3.62966E-07	4.77134E-07
		IWO	3.28266E-06	9.29482E-07	6.38016E-07	8.29738E-07
		TLBO	2.69789E-05	0.000117014	0.000120976	0.000148683
		PSO	8.96172E-13	6.11856E-10	5.51397E-11	1.54776E-10
F11	[-600, 600]	MDE	9.55446E-06	0.169820856	0.055085846	0.054583208
		DE	0.27552729	0.061504309	0.108744396	0.058572068
		IWO	0.036867248	0.273392984	0.11960356	0.080588877
		TLBO	0.039679505	0.192569298	0.128307226	0.077454578
		PSO	0.014779777	0.265798438	0.091004055	0.063259435
F12	[-50, 50]	MDE	1.5816E-26	3.81212E-21	4.29463E-22	1.05256E-21
		DE	9.25465E-15	1.30483E-05	1.09199E-14	3.72369E-15
		IWO	3.72891E-20	4.44482E-15	3.83243E-16	1.14974E-15

		TLBO	3.62368E-16	5.30476E-12	8.24465E-13	1.73365E-12
		PSO	7.55342E-26	2.08922E-19	1.42793E-20	5.38583E-20
F13	[-50, 50]	MDE	1.23159E-21	9.78489E-20	2.46154E-20	2.65061E-20
		DE	3.8418E-22	9.296E-16	1.16986E-15	3.90701E-15
		IWO	3.25238E-19	1.508E-06	3.58863E-07	5.61654E-07
		TLBO	7.17367E-15	5.44348E-06	5.44349E-07	1.72138E-06
		PSO	1.02917E-25	1.12519E-18	8.57027E-20	2.88457E-19

References

- [1] X. Lv, Y. Sun, S. Cao, and V. Dinavahi, "Event-triggered load frequency control for multi-area power systems based on Markov model: A global sliding mode control approach," *IET Gener. Transm. Distrib.*, vol. 14, pp. 4878–4887, Nov. 2020, doi: 10.1049/iet-gtd.2020.0186.
- [2] A. Rafinia, J. Moshtagh, and N. Rezaei, "Towards an enhanced power system sustainability: An MILP under-frequency load shedding scheme considering demand response resources," *Sustain. Cities Soc.*, vol. 59, p. 102168, Aug. 2020, doi: 10.1016/j.scs.2020.102168.
- [3] K. Naidu, H. Mokhlis, and A. H. A. Bakar, "Multiobjective optimization using weighted sum Artificial Bee Colony algorithm for Load Frequency Control," *Int. J. Electr. Power Energy Syst.*, vol. 55, pp. 657–667, Feb. 2014, doi: 10.1016/j.ijepes.2013.10.022.
- [4] M. Kh. AL-Nussairi, S. D. Al-Majidi, A. R. Hussein, and R. Bayindir, "Design of a Load Frequency Control based on a Fuzzy logic for Single Area Networks," in *2021 10th International Conference on Renewable Energy Research and Application (ICRERA)*, Sep. 2021, pp. 216–220. doi: 10.1109/ICRERA52334.2021.9598593.
- [5] F. Mazouz, S. Belkacem, and I. Colak, "DPC-SVM of DFIG Using Fuzzy Second Order Sliding Mode Approach," *Int. J. Smart Grid-IjSmartGrid*, vol. 5, no. 4, pp. 174–82, 2021.
- [6] A. Shahid, "Smart grid integration of renewable energy systems," in *2018 7th International conference on renewable energy research and applications (ICRERA)*, IEEE, 2018, pp. 944–948.
- [7] R. Z. Caglayan, K. Kayisli, N. Zhakiyev, A. Harrouz, and I. Colak, "A review of hybrid renewable energy systems and MPPT methods," *Int. J. Smart Grid-IjSmartGrid*, vol. 6, no. 3, pp. 72–78, 2022.
- [8] S. Pahadasingh, "TLBO based CC-PID-TID controller for load frequency control of multi area power system," in *2021 1st Odisha International Conference on Electrical Power Engineering, Communication and Computing Technology (ODICON)*, IEEE, 2021, pp. 1–7.
- [9] A. Sahu and S. K. Hota, "Performance comparison of 2-DOF PID controller based on Moth-flame optimization technique for load frequency control of diverse energy source interconnected power system," in *2018 Technologies for Smart-City Energy Security and Power (ICSESP)*, IEEE, 2018, pp. 1–6.
- [10] L. C. Saikia and N. Sinha, "Automatic generation control of a multi-area system using ant lion optimizer algorithm based PID plus second order derivative controller," *Int. J. Electr. Power Energy Syst.*, vol. 80, pp. 52–63, 2016.
- [11] D. Guha, P. K. Roy, and S. Banerjee, "Load frequency control of interconnected power system using grey wolf optimization," *Swarm Evol. Comput.*, vol. 27, pp. 97–115, 2016.
- [12] Aditya, "Design of load frequency controllers using genetic algorithm for two area interconnected hydro power system," *Electr. Power Compon. Syst.*, vol. 31, no. 1, pp. 81–94, 2003.
- [13] I. A. Chidambaram and B. Paramasivam, "Optimized load-frequency simulation in restructured power system with redox flow batteries and interline power flow controller," *Int. J. Electr. Power Energy Syst.*, vol. 50, pp. 9–24, 2013.
- [14] Y. Arya and N. Kumar, "Design and analysis of BFOA-optimized fuzzy PI/PID controller for AGC of multi-area traditional/restructured electrical power systems," *Soft Comput.*, vol. 21, pp. 6435–6452, 2017.
- [15] A. Saha and L. C. Saikia, "Utilisation of ultra-capacitor in load frequency control under restructured STPP-thermal power systems using WOA optimised PIDN-FOPD controller," *IET Gener. Transm. Distrib.*, vol. 11, no. 13, pp. 3318–3331, 2017.
- [16] Y. K. Bhatshvar, H. D. Mathur, H. Siguerdidjane, and R. C. Bansal, "Ant colony optimized fuzzy control solution for frequency oscillation suppression," *Electr. Power Compon. Syst.*, vol. 45, no. 14, pp. 1573–1584, 2017.
- [17] S. Vadi, F. B. Gurbuz, S. Sagiroglu, and R. Bayindir, "Optimization of pi based buck-boost converter by particle swarm optimization algorithm," in *2021 9th International Conference on Smart Grid (icSmartGrid)*, IEEE, 2021, pp. 295–301.
- [18] H. R. Chamorro, I. Riano, R. Gerndt, I. Zelinka, F. Gonzalez-Longatt, and V. K. Sood, "Synthetic inertia control based on fuzzy adaptive differential evolution," *Int. J. Electr. Power Energy Syst.*, vol. 105, pp. 803–813, 2019.
- [19] L. Kumar, M. K. Kar, and S. Kumar, "Statistical analysis based reactive power optimization using improved differential evolutionary algorithm," *Expert Syst.*, vol. 40, no. 1, p. e13091, 2023.
- [20] S. Zheng, X. Tang, B. Song, S. Lu, and B. Ye, "Stable adaptive PI control for permanent magnet synchronous motor drive based on improved JITL technique," *Isa Trans.*, vol. 52, no. 4, pp. 539–549, 2013.
- [21] H. Bevrani and P. R. Daneshmand, "Fuzzy logic-based load-frequency control concerning high penetration of wind turbines," *IEEE Syst. J.*, vol. 6, no. 1, pp. 173–180, 2011.
- [22] A. AlKassem, M. Al Ahmadi, and A. Draou, "Modeling and Simulation Analysis of a Hybrid PV-Wind Renewable Energy Sources for a Micro-Grid Application," in *2021 9th International Conference on Smart Grid (icSmartGrid)*, Jun. 2021, pp. 103–106.

- [23] J. Yang, Z. Zeng, Y. Tang, J. Yan, H. He, and Y. Wu, "Load frequency control in isolated micro-grids with electrical vehicles based on multivariable generalized predictive theory," *Energies*, vol. 8, no. 3, pp. 2145–2164, 2015.
- [24] R. R. Kumar, A. K. Yadav, and M. Ramesh, "Hybrid PID plus LQR based frequency regulation approach for the renewable sources based standalone microgrid," *Int. J. Inf. Technol.*, vol. 14, no. 5, pp. 2567–2574, Aug. 2022, doi: 10.1007/s41870-022-01019-3.
- [25] Y. Nagaraja, T. Devaraju, and M. Vijaykumar, "Optimal distributed control of renewable energy-based microgrid – an energy management approach," *Int. J. Ambient Energy*, vol. 42, no. 14, pp. 1635–1642, Oct. 2021
- [26] M. Regad, M. Helaimi, R. Taleb, A. M. Othman, and H. A. Gabbar, "Frequency Control in Microgrid Power System with Renewable Power Generation Using PID Controller Based on Particle Swarm Optimization," in *Smart Energy Empowerment in Smart and Resilient Cities*, M. Hatti, Ed., in Lecture Notes in Networks and Systems. Cham: Springer International Publishing, 2020, pp. 3–13.
- [27] A. Singh and S. Suhag, "Frequency regulation in an AC microgrid interconnected with thermal system employing multiverse-optimised fractional order-PID controller," *Int. J. Sustain. Energy*, vol. 39, no. 3, pp. 250–262, 2020.
- [28] A. Annamraju and S. Nandiraju, "Load frequency control of an autonomous microgrid using robust fuzzy PI controller," in *2019 8th International Conference on Power Systems (ICPS)*, IEEE, 2019, pp. 1–6.
- [29] A. Naderipour, Z. Abdul-Malek, I. F. Davoodkhani, H. Kamyab, and R. R. Ali, "Load-frequency control in an islanded microgrid PV/WT/FC/ESS using an optimal self-tuning fractional-order fuzzy controller," *Environ. Sci. Pollut. Res.*, pp. 1–12, 2021.
- [30] N. K. Jena, S. Sahoo, and B. K. Sahu, "Fractional order cascaded controller for AGC study in power system with PV and diesel generating units," *J. Interdiscip. Math.*, vol. 23, no. 2, pp. 425–434, 2020.
- [31] D. Mishra, M. K. Maharana, and A. Nayak, "Frequency amelioration of an interconnected microgrid system," *Open Eng.*, vol. 12, no. 1, pp. 349–358, 2022.
- [32] M. S. Ayas and E. Sahin, "FOPID controller with fractional filter for an automatic voltage regulator," *Comput. Electr. Eng.*, vol. 90, p. 106895, 2021.
- [33] H. Li, X. Wang, and J. Xiao, "Differential evolution-based load frequency robust control for micro-grids with energy storage systems," *Energies*, vol. 11, no. 7, p. 1686, 2018.
- [34] B. Khokhar, S. Dahiya, and K. S. Parmar, "Load frequency control of a microgrid employing a 2D Sine Logistic map based chaotic sine cosine algorithm," *Appl. Soft Comput.*, vol. 109, p. 107564, 2021.